J. Fluid Mech. (2005), *vol.* 541, *pp.* 105–114.
doi:10.1017/S0022112005006117 Printed in the United Kingdom

Orbiting motion of a freely suspended spheroid near a plane wall

By C. POZRIKIDIS

Department of Mechanical and Aerospace Engineering, University of California, San Diego, La Jolla, CA 92093-0411, USA
cpozrikidis@ucsd.edu

(Received 31 May 2005 and in revised form 6 July 2005)

The effect of a plane wall on the orbiting motion of a freely suspended prolate or oblate spheroidal particle in simple shear flow is described by numerical simulation. The particle translational and angular velocities are computed directly by solving an integral equation of the second kind using a spectral boundary-element method for Stokes flow. The presence of the wall modifies the Jeffery orbits executed by the particle director, and causes the particle centre to perform a lateral and transverse periodic motion deviating from the straight longitudinal path. The effect of the wall is moderate for prolate particles and most significant for oblate particles. In the second case, the complete orbiting motion is suppressed when the particle is sufficiently close to the wall, and the particle director precesses around an axis that is tilted with respect to the vorticity and direction of the simple shear flow, revealing that a neutrally stable steady orientation is established when the particle is in contact with the wall.

1. Introduction

Increasing interest in biological and technological systems involving macromolecules and slender particles in small-scale flows has underscored the significance of particulate hydrodynamics in various contexts, including biomechanics, microfluidics, and materials science. While a wealth of information is available on the motion, interaction, and rheological implications of idealized spherical particles, analytical and computational difficulties have prevented the extensive investigation of disk-like and slender fibre-like particles.

The motion of prolate and oblate ellipsoidal particles suspended in an effectively infinite linear flow at vanishing Reynolds number was described by Jeffery (1922). In one application of the general theory, Jeffery demonstrated that a spheroidal particle suspended in a simple shear flow executes a periodic orbiting motion whose precise trajectory and frequency depend on the particle aspect ratio and initial inclination quantified by the Jeffery constant. Much later, Hsu & Ganatos (1994) performed numerical simulations based on a boundary-integral method to illustrate the effect of a confining boundary idealized as a plane wall. In the numerical studies, freely suspended spheroidal particles convected in simple shear flow, and heavy or light spheroidal particles settling or rising in an otherwise quiescent fluid were considered. In both cases, the particles were oriented such that the flow is left-to-right symmetric with respect to the plane of the particle motion, so that the particle director orbits around a complete circle; in the case of simple shear flow, the particle axis is normal to the vorticity of the simple shear flow. The simulations demonstrated that prolate and

oblate spheroids exhibit a periodic motion in which the particle centre periodically moves away from and toward the wall but does not exhibit a net migration after a complete cycle, as required by reversibility of Stokes flow. Similar calculations were presented by Gavze & Shapiro (1997, 1998). Ellipsoidal particles exhibit a much more complicated dynamics even in the absence of boundaries, including doubly periodic and chaotic orbiting motion (Yarin, Gottlieb & Roisman 1997).

The goal of this paper is to describe the general motion of a freely suspended spheroidal particle in simple shear flow near a plane wall, where the particle axis is tilted by an arbitrary angle with respect to the vorticity of the unperturbed flow. Numerical efficiency is achieved thanks to a problem formulation in terms of a double-layer hydrodynamic potential of Stokes flow, leading to an integral equation of the second kind whose solution can be found accurately and efficiently by the method of successful substitutions combined with a spectral boundary-element expansion. This approach differs from that of previous authors who combined the grand resistance matrix with the condition of zero force and torque to indirectly deduce the particle translational and angular velocity. The numerical results will demonstrate that a confining wall may have a significant effect on the nature of the particle motion in the inclined configuration.

2. Boundary integral formulation

We consider the motion of a rigid particle convected under the influence of a specified incident flow at vanishing Reynolds number. If the particle is neutrally buoyant and the particle inertia negligibly small, the particle motion is quasi-steady and the hydrodynamic force and torque exerted on the particle both vanish. Under these circumstances, the velocity field can be expressed in terms of a double-layer Stokes-flow potential as

$$u_j(\boldsymbol{x}_0) = \boldsymbol{u}_j^{\infty}(\boldsymbol{x}_0) + \iint_D q_i(\boldsymbol{x}) T_{ijk}(\boldsymbol{x}, \boldsymbol{x}_0) \boldsymbol{n}_k(\boldsymbol{x}) \, \mathrm{d}S(\boldsymbol{x}), \tag{2.1}$$

where $\boldsymbol{u}^{\infty}$ is the prescribed velocity field in absence of the particle, D is the particle surface, $\boldsymbol{n}$ is the outward unit normal vector, $\boldsymbol{q}$ is the vectorial strength density of the Stokes double-layer potential represented by the integral on the right-hand side of (2.1), and $T_{ijk}(\boldsymbol{x}, \boldsymbol{x}_0)$ is the Green's function for the stress, known as the stresslet (e.g. Pozrikidis 1992). In the case of flow in infinite space,

$$T_{ijk}(\boldsymbol{x}, \boldsymbol{x}_0) = -6 \frac{\hat{x}_i \hat{x}_j \hat{x}_k}{|\hat{\boldsymbol{x}}|^5}, \tag{2.2}$$

where $\hat{\boldsymbol{x}} = \boldsymbol{x} - \boldsymbol{x}_0$. If the flow is bounded by a solid surface, S_B, $T_{ijk}(\boldsymbol{x}, \boldsymbol{x}_0) = 0$ when $\boldsymbol{x}_0$ lies on S_B, so that the integral representation (2.1) satisfies the boundary condition $\boldsymbol{u}(\boldsymbol{x}_0) = \boldsymbol{0}$ when $\boldsymbol{x}_0$ lies on S_B.

To compute the strength density of the double-layer potential, we let the field point $\boldsymbol{x}_0$ approach the particle surface, D, and express the limit of the double-layer potential in terms of the principal value, denoted by PV, finding

$$u_j(\boldsymbol{x}_0) = u_j^{\infty}(\boldsymbol{x}_0) + 4\pi q_j(\boldsymbol{x}_0) + \iint_D^{PV} q_i(\boldsymbol{x}) T_{ijk}(\boldsymbol{x}, \boldsymbol{x}_0) n_k(\boldsymbol{x}) \, \mathrm{d}S(\boldsymbol{x}). \tag{2.3}$$

Next, we implement the rigid-body-motion boundary condition $\boldsymbol{u} = \boldsymbol{V} + \boldsymbol{\Omega} \times (\boldsymbol{x} - \boldsymbol{x}_c)$, where $\boldsymbol{V}$ is the velocity of translation of the particle centroid defined as

$$\boldsymbol{x}_c \equiv \frac{1}{\mathscr{S}} \iint_D \boldsymbol{x} \, \mathrm{d}S, \tag{2.4}$$

$\mathscr{S}$ is the particle surface area, and $\boldsymbol{\Omega}$ is the angular velocity of rotation about the particle centroid. Rearranging, we derive an integral equation of the second kind for $\boldsymbol{q}$,

$$q_j(\boldsymbol{x}_0) = -\frac{1}{4\pi} \iint_D{}^{PV} q_i(\boldsymbol{x}) T_{ijk}(\boldsymbol{x}, \boldsymbol{x}_0) n_k(\boldsymbol{x}) \, \mathrm{d}S(\boldsymbol{x}) + \frac{1}{4\pi} \left[V_j + \epsilon_{jik} \Omega_i \left(x_{0_k} - x_{c_k} \right) - u_j^{\infty}(\boldsymbol{x}_0) \right]. \tag{2.5}$$

To complete the boundary integral formulation, we stipulate that the translational and rotational velocities derive from the strength density of the double-layer potential as

$$\boldsymbol{V} = -\frac{4\pi}{\mathscr{S}} \iint_D \boldsymbol{q} \, \mathrm{d}S, \qquad \boldsymbol{\Omega} = \sum_{m=1}^{3} d_m \boldsymbol{\omega}^{(m)}, \tag{2.6}$$

where

$$d_m = -\frac{4\pi}{A_m} \boldsymbol{\omega}^{(m)} \cdot \iint_D (\boldsymbol{x} - \boldsymbol{x}_c) \times \boldsymbol{q} \, \mathrm{d}S \tag{2.7}$$

(Pozrikidis 1992, pp. 133–138). The three vectors, $\boldsymbol{\omega}^{(m)}$, are such that

$$\boldsymbol{v}^{(m)} = \frac{1}{\sqrt{A_m}} \boldsymbol{\omega}^{(m)} \times (\boldsymbol{x} - \boldsymbol{x}_c), \tag{2.8}$$

for $m = 1, 2, 3$, are three orthonormal modes of particle rigid-body rotation, that is,

$$\left(\boldsymbol{v}^{(l)}, \boldsymbol{v}^{(m)} \right) \equiv \iint_D \boldsymbol{v}^{(l)} \cdot \boldsymbol{v}^{(m)} \, \mathrm{d}S = \delta_{lm}, \tag{2.9}$$

where δ_{lm} is Kronecker's delta, and

$$A_m = \iint_D \left[\boldsymbol{\omega}^{(m)} \times (\boldsymbol{x} - \boldsymbol{x}_c) \right] \cdot \left[\boldsymbol{\omega}^{(m)} \times (\boldsymbol{x} - \boldsymbol{x}_c) \right] \mathrm{d}S. \tag{2.10}$$

In practice, the vectors $\boldsymbol{\omega}^{(l)}$ can be found by the Gram–Schmidt orthonormalization process. For a spherical particle of radius a, the vectors $\boldsymbol{\omega}^{(l)}$ can be identified with the unit vectors along three Cartesian axes, whereupon $A_m = \frac{8}{3}\pi a^4$ and

$$\boldsymbol{\Omega} = -\frac{3}{2} \left(\frac{4\pi}{\mathscr{S}} \right)^2 \iint_D (\boldsymbol{x} - \boldsymbol{x}_c) \times \boldsymbol{q} \, \mathrm{d}S. \tag{2.11}$$

Finally, a deflating term is added to the right-hand side of (2.5) to yield the modified integral equation

$$q_j(\boldsymbol{x}_0) = -\frac{1}{4\pi} \iint_D{}^{PV} q_i(\boldsymbol{x}) T_{ijk}(\boldsymbol{x}, \boldsymbol{x}_0) n_k(\boldsymbol{x}) \, \mathrm{d}S(\boldsymbol{x}) + \frac{1}{\mathscr{S}} n_j(\boldsymbol{x}_0) \iint_D \boldsymbol{q} \cdot \boldsymbol{n} \, \mathrm{d}S + \frac{1}{4\pi} \left[V_j + \epsilon_{jik} \Omega_i \left(x_{0_k} - x_{c_k} \right) - u_j^{\infty}(\boldsymbol{x}_0) \right]. \tag{2.12}$$

It can be shown that a solution of (2.12) also satisfies (2.5). More important, the deflated integral equation (2.12) can be solved by the method of successive substitutions.

	$\downarrow N_E$	$m \rightarrow$	1	2	3	4	5	Goldman *et al.* (1967)
(*a*)	8	$\hat{V}_x$	0.9404	0.9063	0.9249	0.9276	0.9250	0.9219
	32		0.9348	0.9226	0.9231	0.9227	0.9229	
	8	$\hat{\Omega}_z$	0.7978	0.9320	0.9389	0.9410	0.9422	0.9237
	32		0.8424	0.9244	0.9250	0.9252	0.9250	
(*b*)	8	$\hat{V}_x$	0.7834	0.6958	0.7275	0.7073	0.6669	0.6538
	32		0.7837	0.6908	0.6664	0.6521	0.6533	
	128		0.7262	0.6680	0.6511			
	8	$\hat{\Omega}_z$	0.9126	0.8621	0.8738	0.8039	0.8484	0.6746
	32		0.7997	0.7560	0.6795	0.6622	0.6636	
	128		0.7715	0.7052	0.6681			

TABLE 1. Reduced velocity of translation of the centre of a spherical particle, $\hat{V}_x \equiv V_x/(kd)$, and reduced angular velocity of rotation about the particle centre, $\hat{\Omega}_z \equiv -2\Omega_z/k$, for discretization into $N_E = 8$, 32, and 128 elements defined, respectively, by $N_G = 18$, 66, and 258 geometrical global nodes. Results are shown for several polynomial element expansion orders, m, and for sphere centre to wall separation (*a*) $d/a = 1.5431$, and (*b*) 1.0453.

The deflated integral equation was solved by a spectral-element method, wherein the particle surface is discretized into an unstructured grid of six-node curved triangles, all geometrical variables are approximated with quadratic functions in terms of local triangle (barycentric) coordinates, ξ and η, and the density of the doubly-layer potential, $\boldsymbol{q}$, is approximated with a complete mth-degree polynomial in ξ and η over each element. The associated cardinal interpolation functions are computed from the Proriol orthogonal polynomials using the generalized Vandermonde matrix approach (e.g. Pozrikidis 2005). Finally, point collocation is applied at Lobatto triangle nodes (Blyth & Pozrikidis 2005), and the integral equation is solved by the method of successive substitutions. The singular principal-value integral on the right-hand side of (2.12) was computed by using an integral identity to write

$$\iint_D^{PV} q_i(\boldsymbol{x}) T_{ijk}(\boldsymbol{x}, \boldsymbol{x}_0) n_k(\boldsymbol{x}) \, \mathrm{d}S(\boldsymbol{x}),$$

$$= \iint_D (q_i(\boldsymbol{x}) - q_i(\boldsymbol{x}_0)) T_{ijk}(\boldsymbol{x}, \boldsymbol{x}_0) n_k(\boldsymbol{x}) \, \mathrm{d}S(\boldsymbol{x}) - 4\pi q_j(\boldsymbol{x}_0). \quad (2.13)$$

The non-singular integral containing a mutli-valued integrand on the right-hand side was evaluated by the 9-point Gaussian quadrature for the triangle.

To test the performance of the numerical method, computations were performed for a spherical particle of radius a whose centre is located at a distance d above a stationary plane wall positioned at $y = w$. The requisite Lorentz Green's function is available in terms of image singularities in closed form (Blake 1971; Pozrikidis 1992). The freely suspended particle is convected under the influence of a simple shear flow along the x-axis parallel to the wall, $u_x^\infty = k(y-w)$, $u_y^\infty = 0$, $u_z^\infty = 0$, where k is a specified shear rate. Table 1 lists the computed reduced velocity of translation of the particle centroid, $\hat{V}_x \equiv V_x/(kd)$, and reduced angular velocity of rotation around the z-axis, $\hat{\Omega}_z \equiv -2\Omega_z/k$. As the particle is positioned farther above the wall, $d/a \rightarrow \infty$, both $\hat{V}_x$ and $\hat{\Omega}_z$ tend to unity, corresponding to translation with the velocity of the shear flow evaluated at the particle centroid, and rotation with an angular velocity that is equal

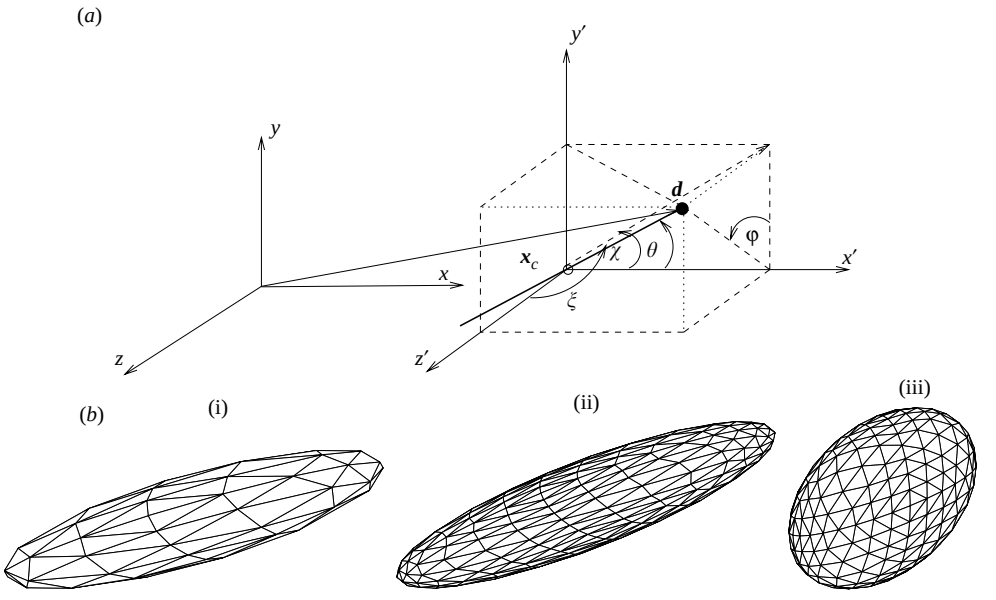

FIGURE 1. (*a*) Illustration of the centreline of a spheroidal particle; (x, y, z) are global Cartesian coordinates, and (x', y', z') are instantaneous coordinates with origin at the particle centre. (*b*) Discretization of the surface of a prolate spheroid with aspect ratio $e = 4$ into (i) 32 or (ii) 128 elements, and of (iii) an oblate spheroid with aspect ratio $e = 0.25$ into 128 elements. For clarity, each quadratic element has been subdivided into four flat sub-elements.

to half the vorticity of the infinite shear flow. Results in table 1 are presented for a moderate particle centre to wall distance, $d/a = 1.5431$, and a smaller distance, 1.0453; both lie outside the lubrication regime. In both cases, the boundary element solution converges rapidly as the order of the polynomial expansion m is raised for a fixed number of elements, N_E, except for the crudest discretization where the numerical integration error is dominant. The last column of table 1 lists values predicted by Goldman Cox & Brenner (1967) using an analytical method. The numerical results for $d/a = 1.5431$ are in good agreement with the theoretical predictions, whereas those for $d/a = 1.0453$ show some differences due to discretization of the particle shape. For the most accurate computations, the combined numerical error due to the particle discretization, double-layer density discretization, and numerical integration is less than 1.0%.

3. Orbiting motion of a spheroid

Our main objective is to describe the motion of a freely suspended spheroidal particle in wall-bounded simple shear flow. The particle position at any instant is determined by the coordinates of the particle centre, $\boldsymbol{x}_c$, and by the orientation of the particle unit director pointing along the particle axis of revolution, $\boldsymbol{d}$, as illustrated in figure 1(*a*). The unit director is a free vector defined by the meridional angle, $\theta = \Theta$, and azimuthal angle, $\varphi = \Phi$, as $d_x = \cos\Theta$, $d_y = \sin\Theta\cos\Phi$, and $d_z = \sin\Theta\sin\Phi$. To reconstruct the particle surface, we generate a spheroid of revolution along the x-axis with centre at the origin, rotate it around the z-axis by the angle Θ, rotate it once again around the x-axis by the angle Φ, and then translate it to the position $\boldsymbol{x}_c$.

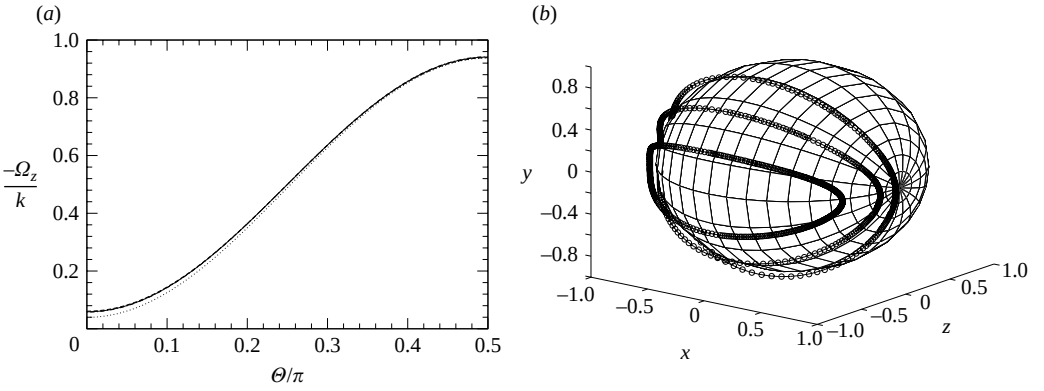

FIGURE 2. (*a*) Angular velocity of rotation of a spheroid with aspect ratio $e = 4$ in the symmetric configuration, $\Phi = 0$, computed with 32 elements and expansion orders $m = 1$, 2, and 3, represented by dotted, dashed, and dot-dashed lines, respectively. The solid line describes Jeffery's exact solution. (*b*) The computed Jeffery orbits marked as circles are in excellent agreement with the analytical results drawn with solid lines threading the circles.

The particle centre translates according to the equation $\mathrm{d}\boldsymbol{x}_c/\mathrm{d}t = \boldsymbol{V}$, and the director angles evolve according to the equations $\mathrm{d}\Theta/\mathrm{d}t = W_\theta$ and $\mathrm{d}\Phi/\mathrm{d}t = W_\varphi/\sin\Theta$, where $\boldsymbol{W} = \boldsymbol{\Omega} \times \boldsymbol{d}$, and

$$\left.\begin{aligned} W_\theta &= -\sin\Theta W_x + \cos\Theta(\cos\Phi W_y + \sin\Phi W_z), \\ W_\varphi &= -\sin\Phi W_y + \cos\Phi W_z. \end{aligned}\right\} \tag{3.1}$$

The initial-value problem defined by these differential equations was integrated in time using the second-order Runge–Kutta method with a constant time step, subject to the initial conditions $\Theta = \pi/2$ and $\Phi = \Phi_0$, where Φ_0 is a specified azimuthal angle. In the most demanding simulations, each time step involving two velocity evaluations requires approximately 10 or 35 s of CPU time on a 2.2 MHz personal computer for a specified sixth-digit numerical threshold in the iterative solution of the integral equation, respectively, for infinite and wall-bounded flow. Only a few iterations are necessary when the initial guess for the solution is the converged solution at the previous step.

Consider the motion of a prolate spheroid with long semi-axis a and short semi-axis b, where $e \equiv a/b > 1$ is the particle aspect ratio. To establish a point of reference and further validate the numerical method, we first discuss the motion of a spheroid with aspect ratio $e = 4$ in infinite simple shear flow. Figure 2(*a*) shows a graph of the angular velocity of rotation around the z-axis plotted against the particle inclination angle, Θ, for the left-to-right symmetric configuration corresponding to $\Phi = 0$. In this computation, the particle surface was discretized into 32 quadratic elements, as illustrated in figure 1(*b*)(i). The dotted, dashed, and dot-dashed lines correspond respectively to element polynomial expansion orders $m = 1, 2$, and 3, and the solid line represents Jeffery's (1922) exact solution described by

$$\Omega_z = \frac{\mathrm{d}\Theta}{\mathrm{d}t} = -\frac{k}{2}\left(1 - \frac{e^2 - 1}{e^2 + 1}\cos(2\Theta)\right). \tag{3.2}$$

In spite of the small number of elements, the numerical results for $m = 2$ and 3 are in excellent agreement with the analytical predictions. Jeffery's formula shows that a spheroid with an infinite aspect ratio, $e = \infty$, remains aligned with the flow in

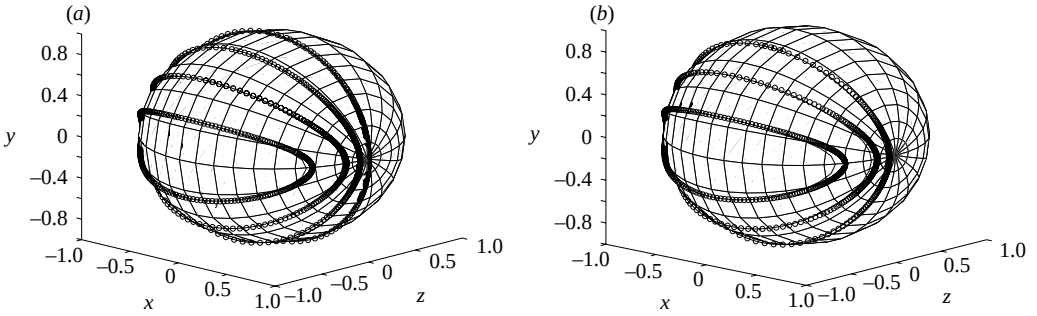

FIGURE 3. Director orbits of a prolate spheroid for particle-centre to wall distance (*a*) $d/a = 1.25$, and (*b*) 1.0. The circular symbols represent the results of the numerical simulations, and the nearly coincident solid lines represent the Jeffery orbits for infinite flow.

the streamwise orientation, $\Theta = 0$, and rotates with angular velocity $\Omega_z = -k$ in the transverse orientation, $\Theta = \pi/2$. The rate of rotation of a prolate spheroid with finite aspect ratio is small when $\Theta = 0$ and highest when $\Theta = \pi/2$.

The circular symbols in figure 2(*b*) trace the orbits of the inclined director computed with 32 elements, element expansion order $m = 2$, and time step $k\Delta t = 0.10$. The hardly visible solid lines threading the data represent Jeffery's analytical predictions described by $d_x = \sin\xi\cos\chi$, $d_y = \sin\xi\sin\chi$, and $d_z = \cos\xi$, where ξ is a meridional angle defined with respect to the z'-axis, and χ is the azimuthal angle subtended between the x'-axis and the projection of the director in the $x'y'$-plane, as shown in figure 1(*a*). The Jeffery orbits are described by $\tan^2\xi(e^2\sin^2\chi + \cos^2\chi) = \mathscr{J}^2$, where the orbital constant $\mathscr{J}$ varies between zero and infinity. When $\Theta = \pi/2$, and correspondingly also $\chi = \pi/2$, the particle axis lies in the $y'z'$-plane, $\xi = \pi/2 - \Phi$ and $\mathscr{J} = e\cot\Phi$. The excellent agreement between the numerical and the analytical results demonstrates the accuracy of the numerical method.

Next, we consider the motion of the prolate spheroid in wall-bounded shear flow. The circular orbit corresponding to $\Phi = 0$ was considered by Hsu & Ganatos (1994) for large and moderate particle-centre to wall separations, $d/a > 2.2$, where d is the distance of the particle centre from the wall in the transverse orientation corresponding to $\Theta = \pi/2$. The present results for this configuration are in good agreement with data read off the graphs of the previous authors, subject to the uncertainty imposed by the narrow plotting window of the published figures. Hsu & Ganatos (1994) tabulate truncated Fourier series approximations for the particle translational and angular velocities in terms of the particle inclination angle, $\alpha = \pi - \Theta$, with an error on the order of 4%. The present results agree with their expressions within this tolerance.

In the simulations presented in the remainder of this section, the particle surface was discretized into 128 isoparametric elements supporting second-order expansions, $m = 2$, and the time step was set to $k\Delta t = 0.10$. Figure 3 illustrates the effect of a plane wall on the Jeffery orbits for particle to wall distance $d/a = 1.25$ and 1.0, as shown in figure 1(*b*)(ii). The circular symbols represent the results of the numerical simulations, and the nearly coincident solid lines represent the Jeffery orbits for infinite flow. Because of the reflection symmetry of the flow with respect to the particle centre, the director orbits remain symmetric with respect to the $y'z'$- and $z'x'$-planes in the presence of the wall. Surprisingly, the wall has only a moderate effect on the director orbits, even when the particle is in close proximity and nearly touches the wall. However, the motion of the particle centre is significantly affected by the presence of the wall.

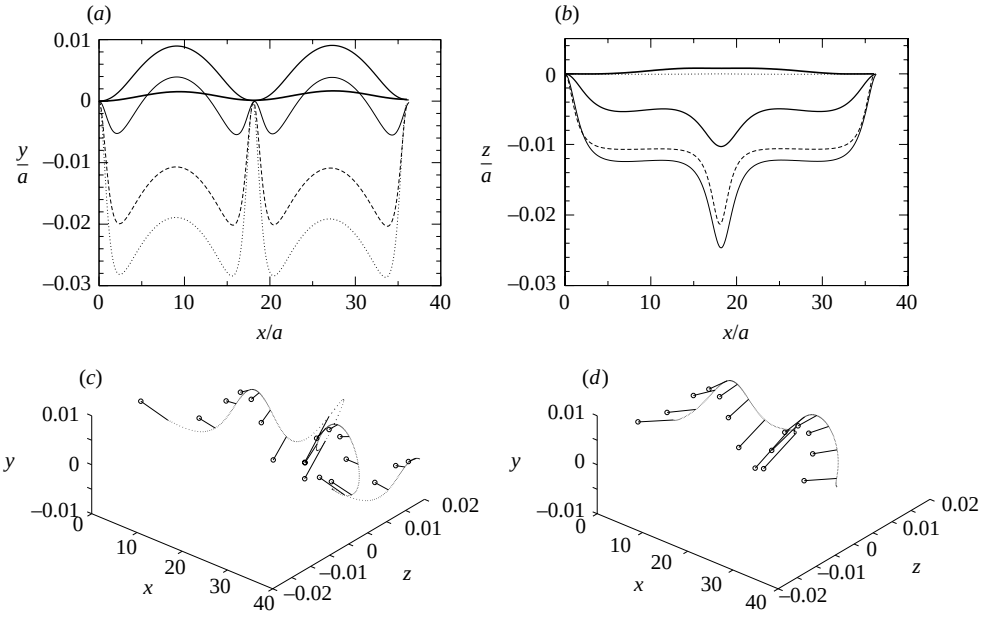

FIGURE 4. (a, b) Projection of particle centre trajectories in the xy- and zx-planes for $d/a = 1.25$, and $\Phi_0/\pi = 0$ (dotted line), 0.125 (dashed line), 0.25 (solid line), 0.375 (thick solid line), and 0.46875 (bold solid line). (c, d) Particle centre trajectory in physical space and evolution of the particle director for Φ_0/π=0.25 and 0.375.

Figure 4(a, b) illustrates the projection of the particle centre trajectories in the xy- and zx-planes for $d/a = 1.25$ and $\Phi_0/\pi = 0$ (dotted line), 0.125, 0.25, 0.375, and 0.46875 (bold solid line). The graphs in figure 4(a) show that the particle centre executes a periodic motion toward and away from the wall depending on the orientation of the long particle axis. As the initial inclination angle Φ_0 tends to $\pi/2$, the long particle axis tends to align with the vorticity of the simple shear flow, the amplitude of the periodic motion is reduced, and the particle motion becomes steady. The graphs in figure 4(b) reveal that a corresponding periodic motion occurs in the transverse direction along the z-axis, except when the initial inclination angle Φ_0 is exactly equal to 0 or $\pi/2$. The nature of the three-dimensional motion is better illustrated in figure 4(c, d), showing the particle center trajectory in physical space with the director visualized as a pin whose sharp end is anchored at the particle centre.

Jeffery (1922) showed that the period of the particle motion in infinite simple shear flow is $T_\infty = (2\pi/k)(e + 1/e)$, independent of the particle tilting angle with respect to the vorticity of the incident shear flow. Figure 5 shows the evolution of the director azimuthal angle, χ, plotted against the reduced time $t' \equiv t/T_\infty$, for particle aspect ratio $e = 4$. Results are shown for $d/a = 1.25$ and $\Phi_0/\pi = 0$, 0.125, 0.25, and 0.375, and for $d/a = 1.0$ and $\Phi_0/\pi = 0.625$, 0.125, 0.25, and 0.375. When $d/a = 1.25$, the wall has only a mild effect on the particle motion for any tilting angle, Φ_0. The effect is small even when the tip of the spheroid is a quarter of the particle major semi-axis away from the wall. At this moderate separation, the period of the motion increases approximately by 10% for any director orbit, due to the wall. The effect becomes more pronounced at the smaller separation $d/a = 1.0$, though even in that case the Jeffery period is only 20% smaller than that occurring in the presence of the wall.

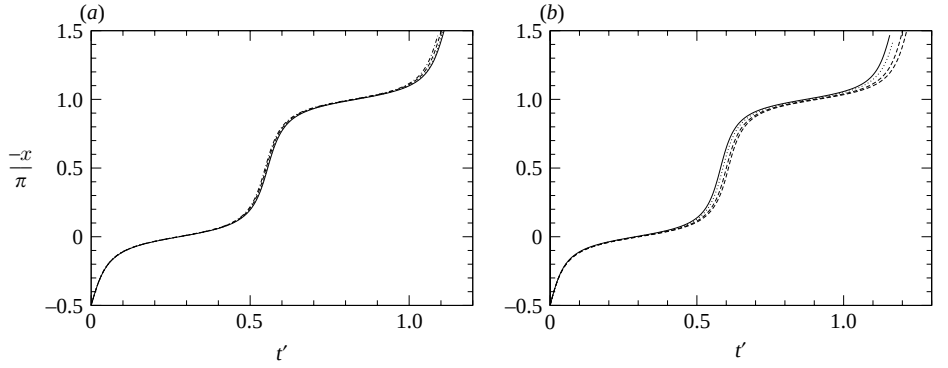

FIGURE 5. Evolution of the director azimuthal angle, χ, with respect to the normalized time $t' \equiv t/T_\infty$, for (*a*) $d/a = 1.25$ and $\Phi_0/\pi = 0.0$, 0.125, 0.25, and 0.375 (solid, dotted, dashed, and dot-dashed lines), and (*b*) $d/a = 1.0$ and $\Phi_0/\pi = 0.0625$, 0.125, 0.25, and 0.375 (solid, dotted, dashed, and dot-dashed lines).

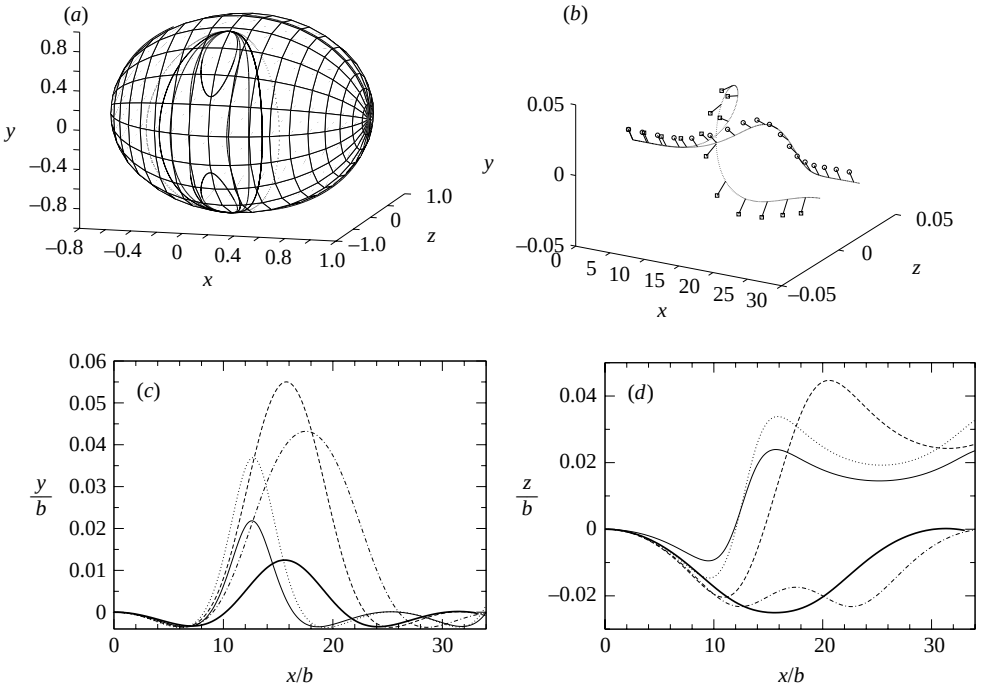

FIGURE 6. (*a*) Director orbit of an oblate spheroid with aspect ratio $e = 0.25$ for initial tilting angle $\Phi_0 = 0.125\,\pi$ in the absence of the wall (dotted line), and for initial particle centre to wall separation $d/b = 1.5$, 1.25, 1.10, and 1.05. (*b*) Particle centre trajectory and evolution of the particle director for $d/b = 1.1$ (square director head) and $d/b = 1.0$ (circular director head). (*c*, *d*) Projection of the particle center trajectories in the xy- and zx-planes for $\Phi_0 = 0.125\,\pi$ and $d/a = 1.5$, (solid lines), 1.25 (dotted lines), 1.1 (dashed lines), 1.05 (dot-dashed lines), and 1.0 (thick solid lines).

Next, we consider the motion of an oblate spheroid with aspect ratio $e = 0.25$. In the left-to-right symmetric configuration corresponding to $\Phi = 0$, the particle director executes a complete circular orbit for any particle to wall separation. Figure 6(*a*) illustrates the effect of the wall on the evolution of the director orbit for initial

particle tilting angle $\Phi_0 = 0.125\,\pi$. The most striking new feature is that, when the particle is close enough to the wall, the complete rotational orbit is suppressed, and the director precesses around an inclined axis. As the particle approaches the wall, a neutrally stable configuration is established wherein the particle moves steadily with its axis tilted by the angle Φ_0 in the plane $\Theta = \pi/2$, while the lower part of the particle surface touches the wall. The transition from full orbital motion to precession occurs at a critical separation, $d/b \simeq 1.055$. At this critical value, the particle tends to turns on its side so that the axis of revolution is aligned with the vorticity of the simple shear flow, so that $\Theta = \pi/2$ and $\Phi = \pi/2$. However, the transverse orientation is unstable and is not expected to occur in practice.

The nature of the motion is illustrated in figure 6(*b*), showing the particle centre trajectory and simultaneous evolution of the particle director for $d/b = 1.0$ and 1.1. In the first case, the particle follows a spiral path, being shifted to the left or to the right depending on the orientation of the director. In the second case, the particle follows a mildly fluctuating wavy path, while the director is always tilted upward. The projection of the particle path in the xy- and zx-planes is shown in figure 6(c, d). The dashed and bold solid lines in these graphs correspond to the two orbits illustrated in figure 6(*b*).

Further simulations for prolate and oblate spheroids of other aspect ratios have revealed similar behaviour. A data base of particle trajectories and director orbits is available from the author on request.

This research was supported by a grant provided by the National Science Foundation.

REFERENCES

Blake, J. R. 1971 A note on the image system for a Stokeslet in a no-slip boundary. *Proc. Camb. Phil. Soc.* **70**, 303–310.

Blyth M. G. & Pozrikidis, C. 2005 A Lobatto interpolation grid on the triangle. *J. Appl Maths.* (in Press).

Gavze, E. & Shapiro, M. 1997 Particles in shear flow near a solid wall: effect of nonsphericity on forces and velocities. *Intl J. Multiphase Flow* **23**, 155–182.

Gavze, E. & Shapiro, M. 1998 Motion of inertial spheroidal particles in a shear flow near a solid wall with special application to aerosol transport in microgravity. *J. Fluid Mech.* **371**, 59–79.

Goldman, A. J., Cox, R. G. & Brenner, H. 1967 Slow viscous motion of a sphere parallel to a plane wall-II Couette flow. *Chem. Engng Sci.* **22**, 653–660.

Hsu, R. & Ganatos, P. 1994 Gravitational and zero-drag motion of a spheroid adjacent to an inclined plane at low Reynolds number. *J. Fluid Mech.* **268**, 267–292.

Jeffery, G. B. 1922 The motion of ellipsoidal particles immersed in a viscous fluid. *Proc. R. Soc. Lond.* A **102**, 161–179.

Pozrikidis, C. 1992 *Boundary Integral and Singularity Methods for Linearized Viscous Flow*. Cambridge University Press.

Pozrikidis, C. 2005 *Introduction to Finite and Spectral Element Methods Using Matlab*. Chapman & Hall/CRC.

Yarin, A. L., Gottlieb, O. & Roisman, L. V. 1997 Chaotic rotation of triaxial ellipsoids in simple shear flow. *J. Fluid Mech.* **340**, 83–100.